science.sciencemag.org/content/371/6528/526/suppl/DC1

Supplementary Materials for

Early plant organics increased global terrestrial mud deposition through enhanced flocculation

Sarah S. Zeichner*, Justin Nghiem, Michael P. Lamb, Nina Takashima, Jan de Leeuw, Vamsi Ganti, Woodward W. Fischer

*Corresponding author. Email: szeichner@caltech.edu

Published 29 January 2021, *Science* **371**, 526 (2021)
DOI: 10.1126/science.abd0379

This PDF file includes:

Materials and Methods

Experimental Design and Construction

Two polymers, xanthan gum (a linear polysaccharide of glucose, mannose, and glucuronic acid produced by the fermentation of plant carbohydrates by the gamma-proteobacterium *Xanthomonas campestris)* and guar gum (a branched polysaccharide of galactose and mannose derived from the plant *Cyamopsis tetragonoloba)*, and two clays, smectite and kaolinite, were used to quantify the effect of organic polymer on flocculation.

Natural soils are dominated by three main types of clay: kaolinite, illite and smectite (*35*); the two clays we chose for this experiment represent mineralogical end members of dominant clay minerals in soils. Kaolinite has 1:1 tetrahedral:octahedral geometry without interlayer cations, whereas smectite has 2:1 tetrahedral:octahedral geometry with charged interlayer cations capable of undergoing distinct bonding interactions with organics.

Likewise, the two polymers chosen for this study have distinct sources, structures, branching patterns, and functional groups that affect presence and abundance within natural soils as well as bonding interactions. At circum-neutral pH, xanthan gum is a negatively charged, linear bacterial polymer, whereas guar gum is a neutral branched plant polymer capable of a wider range of molecular interactions. These molecules are long-chain polysaccharides with variable branches and charged functional groups, comparable to most dominant organic molecules synthesized by plants in their cells walls (e.g., cellulose, (*22*)) and common in soil and sediment environments even as microbes act to degrade and modify plant-derived organic matter (*31*, *36*). With that, we acknowledge the wide diversity of biopolymers present in natural terrestrial organic matter, but used these model polymers as representatives of the most common types of molecules, structures, and functional groups present in plant detritus and the microbes that life closely alongside them, capable of facilitating intramolecular binding interactions. Combinations of these clays and polymers captured a range of potential molecular interactions that occur in natural soils to form flocs in suspended sediment and deposit mud onto floodplains.

Humic acids (*37*) offered another opportunity to test flocculation from plant-derived organic matter, typically generated via incomplete lignin degradation (*37*). Overall, our experiments were designed to optimize the optical quantification of settling velocity for flocs formed by model polymer-clay combinations, and are described below. Humic acid extracts have significant light absorbance at visible wavelengths, so while the results of humic acid experiments were consistent with flocculation behavior demonstrated by xanthan and guar gums, the nature of the humics interfered with the optical absorbance measurements necessary to our primary experimental setup. We applied a distinct approach to facilitate floc tracking and settling velocity calculations in humics experiments: we used kaolinite because of its high contrast and increased the total sediment concentration to 5 g/L with 2.8 weight % humic acid. Note that these sediment concentrations are at the upper range of what is typically observed in rivers (Table S1), and thus preclude direct comparison between humic acid results with our other experiments. However, in experiments where humic extracts were added, we observed formation of kaolinite flocs with diameters of ~100 to 300 μm and settling velocities of ~10^{-3} m/s; experiments with no humics added did not produce any visible flocs.

These experiments gave insight into the complex combination of factors that affect floc formation. Flocculation is driven by primary particle composition and concentration, organic composition, and turbulent shear. In our experiments, we observed that variation in any of these factors yielded measurable differences in flocculation behavior, so we designed the following conditions both to maximize reproducibility among experiments and cover concentration regimes that reflect modern river conditions (Table S1). For each experiment, 0.2 g of clay was weighed into a 500-mL reactor and soaked in distilled water for one (1) hour to ensure full saturation. While soaking, the polymer was weighed to distinct ratios relative to clay weight (1, 2, 5, 8 or 10 weight %) and dissolved in water using a magnetic stir bar. This range of weight percent polymer-to-clay was inspired by the methodology of previous studies of organic-driven freshwater flocculation, and aimed to capture the range of dissolved and particulate organic matter concentrations in modern rivers (*39*, *40*). The concentrations of dissolved and particulate organic matter in paleofluvial systems is not well-constrained beyond the organic contents measured in the resulting sedimentary deposits.

Our experimental setup consisted of a 500-mL batch reactor placed on a stir plate within a light-sensitive box constructed out of aluminum rods (Fig. 2A inset). A light strip was positioned behind the reactor, with a diffusive material placed in front of the light to allow equal distribution of the light throughout the flume for optimal observation of settling. The camera was positioned at a fixed distance on the other side of the settling column within the light-sensitive box to observe the full vertical range of the flume, and connected to an adjacent computer to avoid interaction with the flume or camera during the experiment. The polymer solution and additional water were added to fully fill the 500-mL reactor. The solution was stirred for thirty more minutes prior to observing settling to ensure complete suspension and homogeneous distribution of suspended sediment within the reactor. While turbulence conditions can vary for natural rivers, flow dynamics are thought to be self-similar under the same fully

turbulent flow regime (*41*). We targeted the reactor to be fully turbulent ($Re \sim 10^4$) and set the magnetic stir bar to the identical intensity for each experiment (*42*).

To observe settling, stirring was stopped and photographs were taken using a Nikon D5200 at one-second intervals (Fig. 2A inset). Each photo was cropped to a 198- by 742-pixel matrix to ensure the suspended sediment change over time was calculated over the same interval. To perform the data analysis and characterize the experimental conditions, several control and calibration experiments were performed: First, experiments were performed without addition of organics as a control to characterize behavior of unflocculated clay (e.g., potential for abiotic aggregation). Second, measurements of light intensity were correlated to a range of clay suspended sediment concentration (0.0 g/L to 1.0 g/L, at 0.02 g/L increments), related using an exponential regression, and applied to convert photographs from experiment into concentration units. Third, to constrain the velocity of the water, a buoyant particle was captured moving within the reactor. This value was used to the Reynolds number:

$$Re = \frac{uL}{v}$$

where u is average particle velocity (0.12 m/s), L is the diameter of the reactor (0.08 m), and v is the kinematic viscosity of the fluid (10^{-6} m^2/s). Our flume had an approximate Reynolds number of 10048, and particles followed a chaotic trajectory confirming turbulent flow in our river analog system (*42*). Fourth, to confirm that we were accurately predicting settling velocities in our experimental set-up, we performed calibration experiments with 90 mesh sand (diameter = 165 μm) and compared calculated settling velocities to Stokes' settling estimates (*14*) . Experimental and Stokes' settling velocities for fine-grained sand overlapped within uncertainty. Finally, we performed all of our experiments at least twice to quantify experimental reproducibility. Results from our full set of experiments are presented in Table S2 and the code for photo processing and settling velocity quantification has been made available online (*34*).

Data Analysis and Modeling

Average photo pixel values were used to measure sediment concentration; changes in pixel value over the experiment were converted into sediment concentration over time using a previously determined calibration curve to match pixel intensity to concentration (Fig. S2). Settling velocities were calculated over the interval of maximum settling using the following relationship

$$\frac{C}{C_o} = 1 - \frac{w_s}{\Delta z} t \ (S1)$$

where C is the volumetric suspended sediment concentration of a given area in the photo matrix, C_o is the initial concentration of at that area, w_s is the average settling velocity, Δz is the change in height over the area of interest, and t is time. We fit a line using linear least squares regression between C / C_o and time (e.g., black line in Fig. 2A), and calculated w_s by dividing the best-fit slope of the line by -Δz .

Equation (1) was derived as follows. The change in suspended concentration with respect to time, $\frac{dC}{dt}$, is related to the change in sediment concentration over the height of the cropped photo window dz by mass balance

$$\frac{dC}{dt} = \frac{d(C\, w_s)}{dz} \ (S2)$$

and z is the height of the window of interest, where the z direction is positive upwards. We calculated average concentration using:

$$\bar{C} = \frac{1}{\Delta z} \int_0^{\Delta z} C dz \ (S3)$$

We substituted this relationship into equation (1) to get

$$\frac{d\bar{C}}{dt} = \frac{1}{\Delta z} \left[C w_s|_{z=\Delta z} - C w_s|_{z=0} \right] (S4)$$

The Cw_s term when $z = \Delta z$ is zero because the water at the top of the photo window of interest will clear, and the concentration will go to zero, so

$$\frac{d\bar{C}}{dt} = \frac{-1}{\Delta z} \left[C w_s \right] (S5)$$

Based on the assumption that the settling reached its terminal settling velocity, we integrated the two sides of the equation with respect to concentration and time to find equation (S1), using the initial concentration at t = 0 is the initial sediment concentration C_o.

Statistical analysis

We grouped our average measured settling velocities to evaluate statistically significant differences between the settling velocities observed under different experimental conditions. We formally tested the following null hypotheses H_0, with rows of Table S2 indicated in parentheses, to indicate which experiments were used for each test.

(1) The addition of organics produced identical average clay settling velocities compared to clay without organics added (control: 1, 12; flocculated: 2:11, 13:29).
(2) The addition of guar gum yielded identical average floc settling velocities compared to those produced via the addition of xanthan gum (guar: 2:6, 13:17, 23:26; xanthan 7:11, 18:22, 27:29).
(3) The guar gum-smectite combination produced flocs with identical average settling velocities compared to those produced by any other polymer-clay combination (smectite-guar: 2:6, 23:26; everything else: 7:22, 27:29)

For each hypothesis, we tested an alternative hypothesis H_a in which the first group (i.e., "addition of organics" for hypothesis 1) produced greater settling velocities. Thus, we performed *t*-tests with H_0: $\mu = \mu_0$ and H_a: $\mu > \mu_0$. *p*-values were reported based on Welch's two-sample, one-sided *t*-tests using the "t.test" function in the R statistical software (www.r-project.org).

Floodplain sedimentation model

We modeled overbank flow using a one-dimensional floodplain cross-sectional profile perpendicular to a river channel, with deposition rates of sediment input spanning clay to sand sizes (Fig. 3A). The spatial domain we considered was half of a floodplain on one side of the channel. The model is a suspended sediment advection-settling model, similar to models derived in previous work (*43*), and is derived in a simple form to arrive at an analytical solution.

The mass conservation of suspended sediment in one dimension is

$$\frac{\partial q_s}{\partial x} = w_s(e_s - C_b) \ (S6)$$

in which q_s is the volumetric sediment flux per unit width (m^2/s), x is the horizontal distance across the floodplain from the channel edge (m), w_s is particle settling velocity (m/s), e_s is the dimensionless entrainment rate from the bed, and C_b is the dimensionless near-bed volumetric sediment concentration (*44*, *45*). The sediment transport parameters are grain size-specific, and the generalization to many grain sizes was made in our implementation.

We assumed that sediment entrainment on the floodplain was negligible, and that sediment transport occurred due to advection without turbulent diffusion. These conditions gave $e_s = 0$ and $q_s = \bar{C}q$, respectively, where $\bar{C}$ is the depth-averaged dimensionless volumetric sediment concentration and q is the overbank water discharge per unit width (m^2/s). We used $r_0 \equiv \frac{C_b}{\bar{C}} \geq 1$ to describe the stratification of the vertical suspended sediment concentration profile (*44*). Using these assumptions and definitions, we integrated Eq. (S6) to find

$$\bar{C}(x) = C_0 \exp\left(-\frac{w_s r_0}{q}x\right) \ (S7)$$

in which the sediment concentration at the boundary of the channel and floodplain is C_0. We differentiated equation (S7) with respect to x and multiplied both sides by q to recover an equation for the divergence in sediment flux

$$\frac{\partial q_s}{\partial x} = -w_s r_0 C_0 \exp\left(-\frac{w_s r_0}{q}x\right) \ (S8)$$

The divergence of the sediment flux is related to changes in floodplain elevation using the Exner conservation of sediment mass equation

$$(1 - \lambda_p)\frac{\partial \eta}{\partial t} = -\frac{\partial q_s}{\partial x} \ (S9)$$

where λ_p is the porosity of the sediment deposit, η is floodplain elevation, and t is time (*46*). Substituting equation (S8) into equation (S9) results in an expression for the floodplain aggradation rate

$$\frac{\partial \eta_i}{\partial t} = \frac{w_{si} r_0 C_{0i}}{1 - \lambda_p} \exp\left(-\frac{w_{si} r_0}{q}x\right) \text{(S10)}$$

where the subscript *i* denotes values for the *i*th grain-size class when generalizing to *n* grain-size classes. We assumed that the parameters on the right-hand side of equation (S10) do not vary significantly with time during a characteristic flood event.

Inspection of equation (S10) revealed that flocculation leads to faster floodplain mud deposition rates, all else being equal. Across different fluvial systems, overbank discharge, sediment concentration, and grain size distribution can vary and cause different deposition rates and spatial trends in grain size composition of deposits. For any given combination of those variables, flocculation increases settling velocities w_{si} for mud particles. Based on

equation (S10), higher mud settling velocities led to two interacting effects: first, $\frac{\partial \eta}{\partial t}$ increases linearly with w_{si} and second, $\frac{\partial \eta}{\partial t}$ decays exponentially with w_{si} where the horizontal scale is also determined by overbank discharge q. Thus, flocculation causes overall greater mud aggradation rates, and a steeper falloff of mud deposition rate with distance from the channel.

Input model parameters for two scenarios were scaled after observed values for the Mississippi River, USA as an example of a large, low-gradient fluvial system (*47*, *48*), which exemplifies the deep channeled, low-gradient single-threaded rivers common before and after the Silurian Period (*23*). The per-width discharge q is the product of overbank flow depth and velocity. We based overbank flow depth of 2.3 m and overbank flow velocity of 1 m/s (q = 2.3 m^2/s) on direct flood measurements at the main stem Missouri River near its confluence with the Mississippi River (*49*). The total overbank sediment concentration sourced from the channel, which sets $C_0 = \sum C_{0i}$, is independent of percent mud and normalized deposition rate, so it was set to an arbitrary constant. We specified a log-normal distribution of suspended sediment grain size at the channel boundary (median or geometric mean 5.6 μm, geometric standard deviation 5.5 mm) to interpolate the total averaged concentration across 28 log-spaced size classes with minimum grain size 0.02 μm and maximum grain size 2 mm (Fig. 3A). For the flocculated mud scenario, all grains smaller than 20 μm were considered flocculated to a uniform floc settling velocity of 0.34 mm/s (Fig. 3B) following the estimated average floc settling velocity in modern rivers based on analysis of river suspended sediment concentration profiles (*10*). Although suspended sediment may be flocculated for grains up to 40 μm (*10*), Stokes' settling velocity predictions exceed 0.34 mm/s for grains larger than 20 μm (*50*). Thus, a uniform settling velocity of 0.34 mm/s was only assigned to those grain size classes smaller than 20 μm to enforce the observation that flocculation generally increases settling velocity. Compared to the experiment results, the prescribed floc settling rate of 0.34 mm/s was similar to the estimated settling velocity in the 2 and 5% weight ratio smectite-guar treatment (0.265 and 0.437 mm/s, respectively; Fig. 2C), and fell in the range of experiment settling velocities. Based on prior work, we expected that the presence of silt, which we did not explicitly test in experiments, would further increase floc settling velocities (*20*). For coarser grains and all grains in the unflocculated case, settling velocity was calculated from reference (*50*). We specified $r_0 = 1$ (corresponding to a uniform suspended sediment concentration profile) because the influence of r_0 was of secondary importance compared to the settling velocity.

We generated the grain size-specific floodplain model profiles according to equation (S10), and used the model profiles to assess the effect of flocculation on relative mud abundance compared to sand across a floodplain (Fig. 3C). We classified and aggregated these results into mud (D < 62.5 μm) and sand (D > 62.5 μm) size classes to calculate percent mud of deposits (Fig. 3C). Fig. 3C shows the proximal floodplain over a width of twice the advection length of sand particles (~170 m) to maintain appreciable sand in the domain for comparison with mud deposition (Fig. 3C). The advection length is the characteristic length over which a particle of a given size is transported before it settles to the bed in the absence of entrainment, and can be calculated from the per-width water discharge q divided by the settling velocity w_s of the median sand grain size (*43*). This formulation illustrated that q controls the horizontal spatial scale of deposition, and that changing the value of q directly changed the scale of floodplain length at a fixed channel position but did not change the relative distribution of mud and sand. Beyond twice the advection length, the prevalence of mud over sand became more associated with the inability of the flow to transport sand grains and less due to the effects of flocculation. In other words, percent mud tended to unity with distance from the channel for all cases for large transport distances (many times the advection length of sand) simply because the sand fraction settled out completely.

Figure 3D shows the predictions of equation (S10) over a much greater distance across the floodplain. We used equation (S10) to compare relative magnitudes of mud deposition rates across a floodplain for flocculated and unflocculated scenarios (Fig. 3D). We summed deposition rates for mud size classes to compute the total mud deposition rate. We normalized the deposition rates by the maximum deposition rate in the flocculated case (occurring at the channel bank, x = 0) to better highlight the comparison.

In order to generalize the model results to fluvial settings beyond that considered here, we varied the input parameters independently to demonstrate their effects on the results across ranges of plausible values (Fig. S4). Specifically, the input parameters of per-width overbank discharge q, grain size distribution of suspended sediment advected from the channel, and floc settling velocity $w_{s,\,\mathrm{floc}}$ determine the two model results, percent mud and normalized mud deposition rate (Fig. 3C and 3D). We characterized variations in grain size distribution as variations in the median of the distribution D_{50} and held the standard deviation constant. While the lowland alluvial setting considered in Fig. 3 is likely to deposit substantial mud and preserve mudrock in the rock record, other types of river systems with different planform geometries and/or gradients can yield different model results because of correlated trends with characteristic overbank discharges, suspended sediment grain size distribution and floc settling velocity.

Using the flocculated scenario inputs and results from Fig. 3 as a base case, we calculated percent mud and normalized mud deposition rate for each parameter of interest (q, D_{50}, and $w_{s,\,floc}$) by varying that parameter across realistic natural values and setting all other parameters to the same values used in the flocculated base case. We then compared each modeled scenario to an equivalent unflocculated scenario by setting sediment settling velocities according to predictions (*50*). As a result, these tests demonstrated the likely range of model outcomes that can be associated with variations in physical properties of rivers.

The model sensitivity results for all variables demonstrated that individual variations in these parameters always produce sand-mud transitions closer to the channel compared to unflocculated scenarios (Fig. S4). This result was consistent with the generation of muddier floodplains caused by mud flocculation. Similarly, mud deposition rate results showed that, in most cases, mud deposition rate in a distal location from the channel can be increased by up to tenfold compared to unflocculated cases, again consistent with muddier floodplains. However, deposition rate of flocculated mud can be smaller than that of unflocculated mud for sufficiently small $q < 1$ m^2/s. This behavior highlighted the role of q in setting the horizontal mud advection scale. If discharge is too small, the flocculated mud will settle out completely closer to the channel such that more distal parts of the floodplain will be starved of mud. Additionally, model results for large D_{50} converged to the unflocculated case, showing that the effect of flocculation is minimal with low mud supply from the channel.

If we considered for model purposes that different fluvial systems are characterized by differences in their overbank discharge and sediment grain size distribution and that flocculation simply sets the grain size-settling velocity relationship, then the introduction of mud flocculation always produced a model response for any given river tending to muddier floodplains for realistic ranges of $w_{s,\,floc}$ (Fig. S4). Compared to unflocculated results at identical discharge and grain size distribution, $w_{s,\,floc}$ promoted higher distal floodplain mud deposition rates (up to 3.6 times greater than that of the unflocculated case) and more proximal transitions to dominantly mud deposits (up to 2 orders of magnitude closer to the channel). Thus, the role of mud flocculation alone is expected to cause more channel-proximal floodplain mud distribution and greater floodplain mud abundance, and in turn overall muddier floodplains.

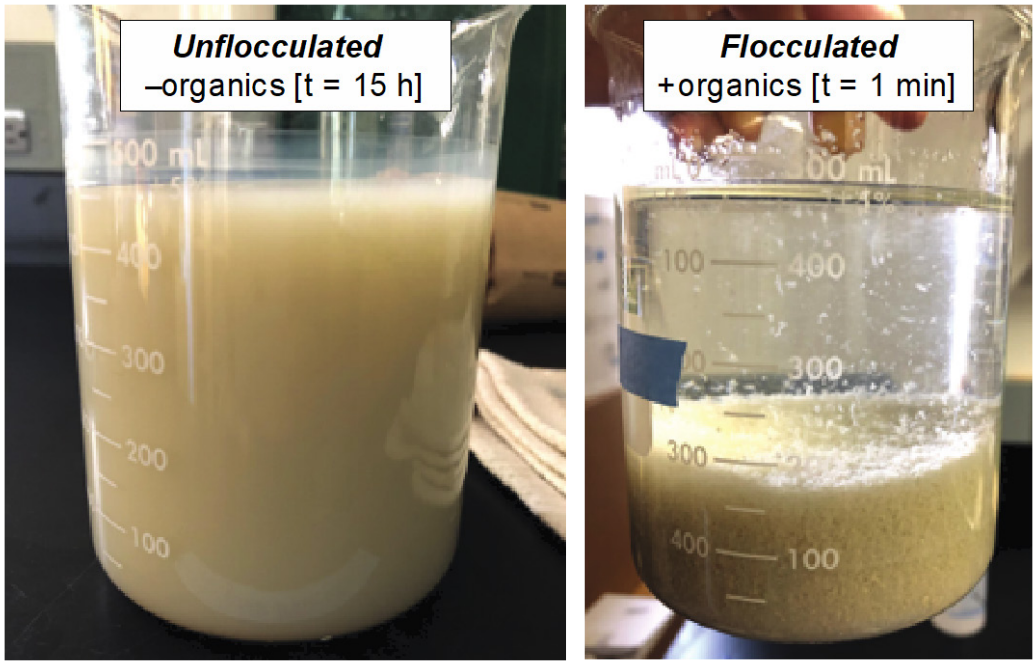

Fig. S1. Flocculated and unflocculated clays. Example of the substantial impact that organic polymers can have on flocculation and settling. Unflocculated smectite (2 g/500 mL) in optical settling column after sitting overnight (left) versus flocculated, settled smectite (2 g/500 mL + 1 weight % guar gum) after t = 1 minute (right).

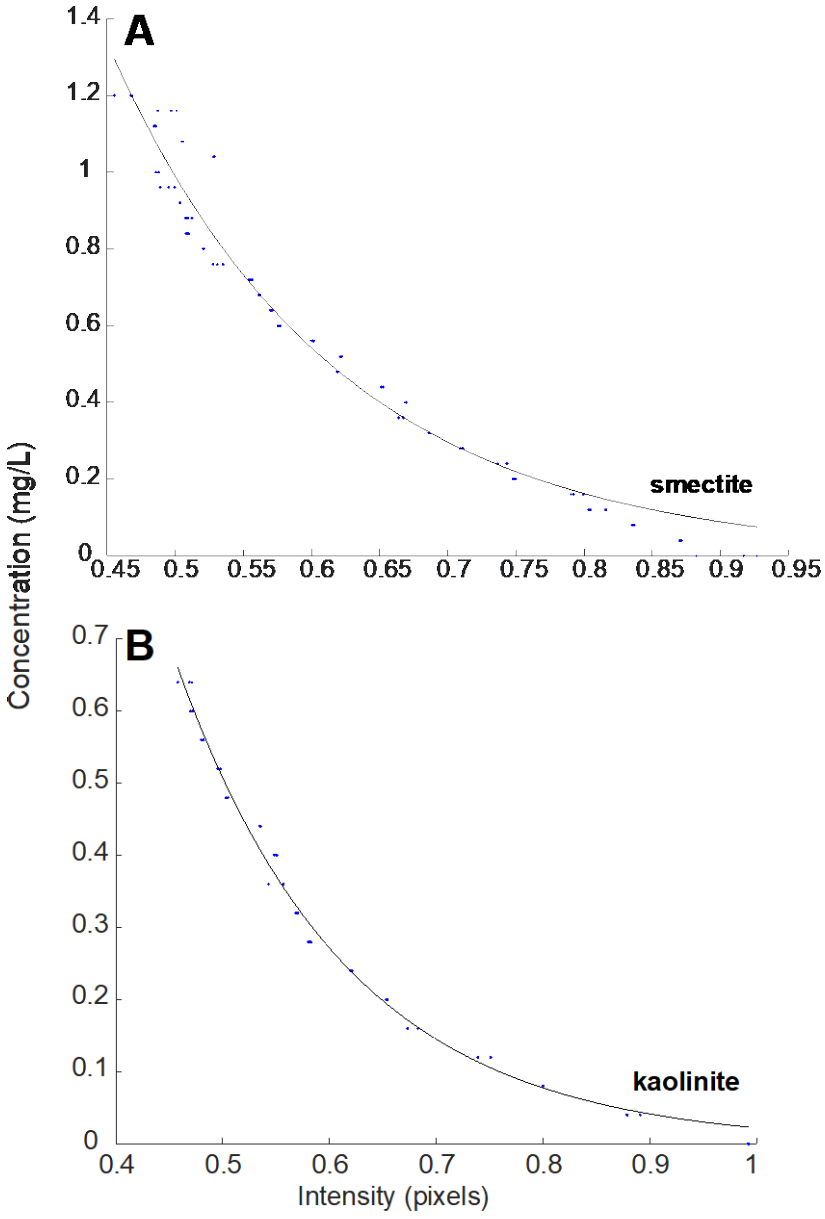

Fig. S2. Experimental intensity to sediment concentration calibration curves. Calibration curves for (A) smectite and (B) kaolinite that were used to calculate light absorbance (measured by photo pixel intensity) into sediment concentration.

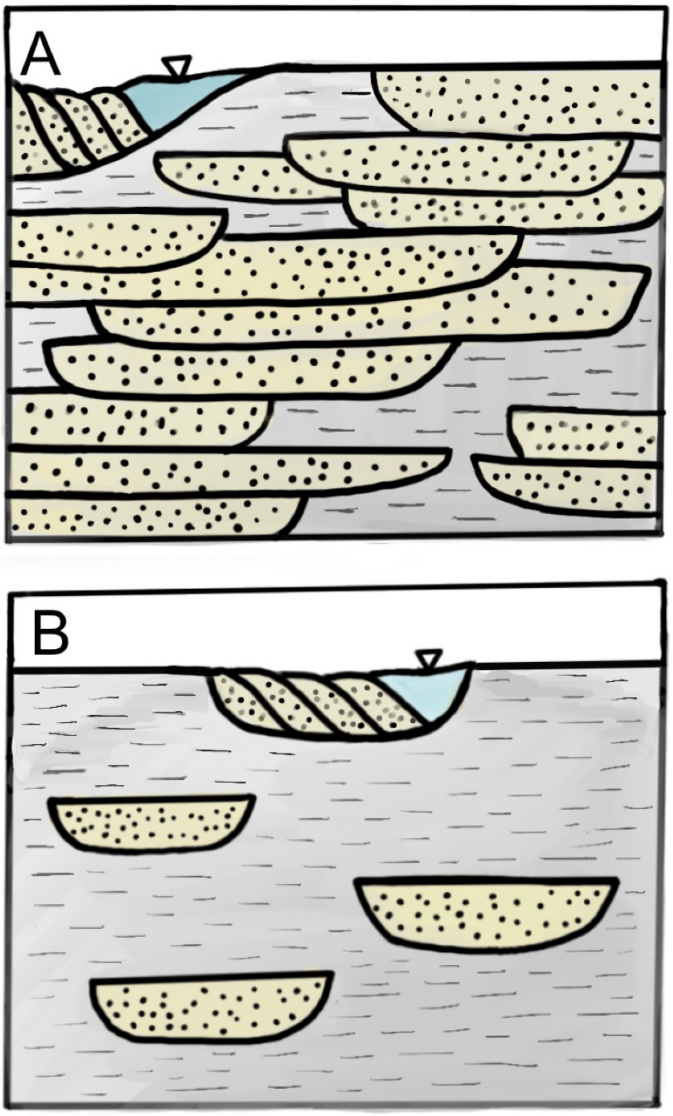

Fig. S3. Sand- versus mud-dominant alluvial deposits. Schematic showing the potential distribution of mud and sand within fluvial deposits (A) without and (B) with flocculation, driven by different amounts lateral channel migration relative to avulsion. Without flocculation, banks are sandier and river lateral migration rates are faster, resulting in wider sand bodies that are more interconnected. With flocculation, banks are stronger and channel bodies are narrower, and reduced lateral migration relative to avulsion results in isolated sandstone bodies.

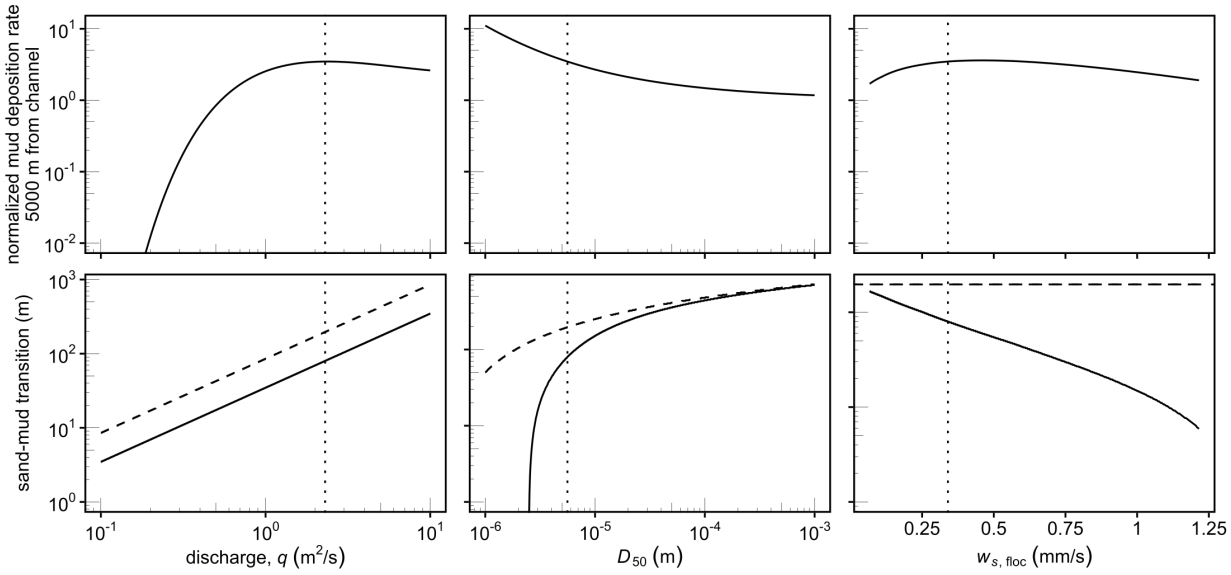

Fig. S4. Floodplain sediment transport model sensitivity analysis. Model results showing the effect of overbank discharge per unit width, q, median grain size, D_{50}, and floc settling velocity $w_{s,\,floc}$ (range of 16th to 84th percent quantiles of $w_{s,\,floc}$ based on modern river data analyzed in (*10*)) on the main results shown in Fig. 3. Top row: Mud deposition rate on the floodplain at 5000 m from the channel for the flocculated case, normalized by mud deposition rate at 5000 m for the unflocculated case. Bottom row: Distance from the channel of the sand-mud transition (defined by 50% mud). The dashed curves in the bottom row panels mark the distance of the sand-mud transition in the unflocculated case calculated with Stokes' settling velocities. For each column, all other variables in the model were held constant and set to the values used in Fig. 3 (q = 2.3 m^2/s, D_{50} = 5.6 μm, $w_{s,\,floc}$ = 0.34 mm/s, shown as vertical dotted lines in their respective columns).

Attribute	Observed condition
Suspended sediment concentrations	0.14 – 3.08 g/L, average of 1.25 g/L (*38*)
Most abundant clay minerals	Illite, kaolinite, smectite, vermiculite (*35*)
Organic concentrations	1-6%(*19*); 1-20%(*9*)

Table S1. Typical natural river conditions. Relevant characteristics of global river sediment that guided experimental design for the flocculation experiments. Continents vary in clay mineralogy and percentage due to soil type, topography, and bedrock geology. The ranges for percent organics were based on two studies examining the role of organics in forming flocs within fluvial systems.

	Clay	Polymer	E/C (%)	n	Absolute value of settling velocity (abs(velocity), m/s)	Relative standard error	log_{10}(abs(velocity))
1	Smectite	n/a	0	9	1.69E-06	1.57E+00	-5.77
2	Smectite	guar	1	5	6.24E-05	4.06E-01	-4.20
3	Smectite	guar	2	4	2.65E-04	5.21E-01	-3.58
4	Smectite	guar	5	11	4.37E-04	1.96E-01	-3.36
5	Smectite	guar	8	3	6.28E-04	2.43E-01	-3.20
6	Smectite	guar	10	4	1.28E-03	2.48E-01	-2.89
7	Smectite	xanthan	1	3	1.55E-06	-2.77E+01	-5.81
7	Smectite	xanthan	2	3	2.40E-06	-1.74E+00	-5.62
8	Smectite	xanthan	5	2	1.24E-05	6.75E-01	-4.91
9	Smectite	xanthan	8	3	3.37E-06	3.22E-02	-5.47
10	Smectite	xanthan	10	3	3.19E-06	-7.49E-01	-5.50
11	Kaolinite	n/a	0	3	2.72E-06	6.36E-07	-5.57
12	Kaolinite	guar	1	4	1.54E-05	2.47E-01	-4.81
13	Kaolinite	guar	2	3	2.64E-05	7.36E-01	-4.58
14	Kaolinite	guar	5	2	6.20E-06	2.90E+00	-5.21
15	Kaolinite	guar	8	2	3.99E-06	-2.84E-01	-5.40
16	Kaolinite	guar	10	2	3.32E-06	-2.96E-01	-5.48
17	Kaolinite	xanthan	1	2	1.82E-05	-1.19E-01	-4.74
18	Kaolinite	xanthan	2	2	7.44E-06	3.29E-01	-5.13
19	Kaolinite	xanthan	5	2	1.33E-05	-5.70E-01	-4.88
20	Kaolinite	xanthan	8	1	6.93E-06	n/a	-5.16
21	Kaolinite	xanthan	10	2	8.59E-06	-1.78E-01	-5.07
22*	Kaolinite	humic	2.8	2	1E-03	2E-04	-3
23	Smectite : Kaolinite (0.25)	guar	10	1	8.72E-05	n/a	-4.06
24	Smectite : Kaolinite (0.50)	guar	5	1	6.34E-04	n/a	-3.20

25	Smectite : Kaolinite (0.50)	guar	10	1	4.63E-04	n/a	-3.33
26	Smectite : Kaolinite (0.75)	guar	10	1	6.44E-04	n/a	-3.19
27	Smectite : Kaolinite (0.50)	xanthan	2	1	3.17E-06	n/a	-5.50
28	Smectite : Kaolinite (0.50)	xanthan	5	1	3.61E-05	n/a	-4.44
29	Smectite : Kaolinite (0.50)	xanthan	10	1	8.59E-06	n/a	-5.07
30	90 Mesh sand	n/a	n/a	3	1.72E-02	3.54E-01	-1.76
31	Fine silt (theoretical)	n/a	n/a	n/a	1.44E-06	n/a	-5.84
32	Coarse silt (theoretical)	n/a	n/a	n/a	1.44E-04	n/a	-3.84
33	Fine Sand (theoretical)	n/a	n/a	n/a	2.29E-02	n/a	-1.64

Table S2. Experimental results. Settling velocities measured in flocs experiments. Italicized rows represent settling velocities that were not meaningfully different from the clay control when accounting for the uncertainty in the sediment concentration measurements. The asterisk denotes distinct experimental setup used for humic acid experiment.

References and Notes

1. C. K. Boyce, J.-E. Lee, Plant evolution and climate over geological timescales. *Annu. Rev. Earth Planet. Sci.* **45**, 61–87 (2017). doi:10.1146/annurev-earth-063016-015629

2. D. Long, "Proterozoic stream deposits: Some problems of recognition and interpretation of ancient sandy fluvial systems" in *Fluvial Sedimentology—Memoir 5*, A. D. Miall Ed. (Canadian Society of Petroleum Geologists, 1978), pp. 313–341.

3. W. J. McMahon, N. S. Davies, Evolution of alluvial mudrock forced by early land plants. *Science* **359**, 1022–1024 (2018). doi:10.1126/science.aan4660 Medline

4. N. S. Davies, M. R. Gibling, Cambrian to Devonian evolution of alluvial systems: The sedimentological impact of the earliest land plants. *Earth Sci. Rev.* **98**, 171–200 (2010). doi:10.1016/j.earscirev.2009.11.002

5. W. W. Fischer, Early plants and the rise of mud. *Science* **359**, 994–995 (2018). doi:10.1126/science.aas9886 Medline

6. R. Hadley, "Influence of riparian vegetation on channel shape, northeastern Arizona" (Geological Survey Professional Paper 424–C, U.S. Government Printing Office, 1961), pp. 30–31.

7. S. McMahon, J. Parnell, The deep history of Earth's biomass. *J. Geol. Soc. London* **175**, 716–720 (2018). doi:10.1144/jgs2018-061

8. F. Maggi, "Flocculation dynamics of cohesive sediment," thesis, Delft University of Technology (2005).

9. G. Zhang, H. Yin, Z. Lei, A. H. Reed, Y. Furukawa, Effects of exopolymers on particle size distributions of suspended cohesive sediments. *J. Geophys. Res. Oceans* **118**, 3473–3489 (2013). doi:10.1002/jgrc.20263

10. M. P. Lamb, J. De Leeuw, W. Fischer, A. J. Moodie, J. Venditti, J. Nittrouer, D. Haught, G. Parker, Mud is transported as flocculated and suspended bed material. *Nat. Geosci.* **13**, 566–570 (2020). doi:10.1038/s41561-020-0602-5

11. E. R. Sholkovitz, Flocculation of dissolved organic and inorganic matter during the mixing of river water and seawater. *Geochim. Cosmochim. Acta* **40**, 831–845 (1976). doi:10.1016/0016-7037(76)90035-1

12. Y. Furukawa, A. H. Reed, G. Zhang, Effect of organic matter on estuarine flocculation: A laboratory study using montmorillonite, humic acid, xanthan gum, guar gum and natural estuarine flocs. *Geochem. Trans.* **15**, 1–9 (2014). doi:10.1186/1467-4866-15-1 Medline

13. See supplementary materials.

14. G. G. Stokes, On the effect of internal friction of fluids on the motion of pendulums. *Trans. Cambridge Philos. Soc.* **9**, 8–106 (1851).

15. X. L. Tan, G. P. Zhang, H. Yin, A. H. Reed, Y. Furukawa, Characterization of particle size and settling velocity of cohesive sediments affected by a neutral exopolymer. *Int. J. Sediment Res.* **27**, 473–485 (2012). doi:10.1016/S1001-6279(13)60006-2

16. J. Námer, J. J. Ganczarczyk, Settling properties of digested sludge particle aggregates. *Water*

Res. **27**, 1285–1294 (1993). doi:10.1016/0043-1354(93)90215-4

17. W. Lick, H. Huang, R. Jepsen, Flocculation of fine-grained sediments due to differential settling. *J. Geophys. Res.* **98**, 10279 (1993). doi:10.1029/93JC00519

18. Q. Q. Shang, H. W. Fang, H. M. Zhao, G. J. He, Z. H. Cui, Biofilm effects on size gradation, drag coefficient and settling velocity of sediment particles. *Int. J. Sediment Res.* **29**, 471–480 (2014). doi:10.1016/S1001-6279(14)60060-3

19. V. Wendling, N. Gratiot, C. Legout, I. G. Droppo, C. Coulaud, B. Mercier, Using an optical settling column to assess suspension characteristics within the free, flocculation, and hindered settling regimes. *J. Soils Sediments* **15**, 1991–2003 (2015). doi:10.1007/s11368-015-1135-1

20. D. Tran, K. Strom, Suspended clays and silts: Are they independent or dependent fractions when it comes to settling in a turbulent suspension? *Cont. Shelf Res.* **138**, 81–94 (2017). doi:10.1016/j.csr.2017.02.011

21. M. Pauly, K. Keegstra, Plant cell wall polymers as precursors for biofuels. *Curr. Opin. Plant Biol.* **13**, 305–312 (2010). doi:10.1016/j.pbi.2009.12.009 Medline

22. Z. A. Popper, Evolution and diversity of green plant cell walls. *Curr. Opin. Plant Biol.* **11**, 286–292 (2008). doi:10.1016/j.pbi.2008.02.012 Medline

23. V. Ganti, A. C. Whittaker, M. P. Lamb, W. W. Fischer, Low-gradient, single-threaded rivers prior to greening of the continents. *Proc. Natl. Acad. Sci. U.S.A.* **116**, 11652–11657 (2019). doi:10.1073/pnas.1901642116 Medline

24. M. G. A. Lapôtre, A. Ielpi, M. P. Lamb, R. M. E. Williams, A. H. Knoll, Model for the formation of single-thread rivers in barren landscapes and implications for pre-Silurian and Martian fluvial deposits. *J. Geophys. Res. Earth Surf.* **124**, 2757–2777 (2019). doi:10.1029/2019JF005156

25. D. J. Jerolmack, D. Mohrig, Conditions for branching in depositional rives. *Geology* **35**, 463–466 (2007). doi:10.1130/G23308A.1

26. V. Ganti, E. A. Hajek, K. Leary, K. M. Straub, C. Paola, Morphodynamic hierarchy and the fabric of the sedimentary record. *Geophys. Res. Lett.* **47**, 1–10 (2020). doi:10.1029/2020GL087921

27. D. Winston, "Fluvial systems of the Precambrian Belt Supergroup, Montana and Idaho, U.S.A." in *Fluvial Sedimentology—Memoir 5*, A. D. Miall, Ed. (Canadian Society of Petroleum Geologists, 1978), p. 343.

28. E. Cotter, "The evolution of fluvial style, with special reference to the Central Appalachian Paleozoic" in *Fluvial Sedimentology—Memoir 5*, A. D. Miall, Ed. (Canadian Society of Petroleum Geologists, 1978), pp. 361–383.

29. A. Ielpi, P. Fralick, D. Ventra, M. Ghinassi, L. E. Lebeau, A. Marconato, R. Meek, R. H. Rainbird, Fluvial floodplains prior to greening of the continents: Stratigraphic record, geodynamic setting, and modern analogues. *Sediment. Geol.* **372**, 140–172 (2018). doi:10.1016/j.sedgeo.2018.05.009

30. D. Edwards, L. Cherns, J. A. Raven, Could land-based early photosynthesizing ecosystems

have bioengineered the planet in mid-Palaeozoic times? *Palaeontology* **58**, 803–837 (2015). doi:10.1111/pala.12187

31. M. V. Cheshire, Origins and stability of soil polysaccharide. *J. Soil Sci.* **28**, 1–10 (1977). doi:10.1111/j.1365-2389.1977.tb02290.x

32. J. R. Hatch, G. B. Morey, Hydrocarbon source rock evaluation of Middle Proterozoic Solor Church Formation, North American Mid-Continent Rift System, Rice County, Minnesota. *Am. Assoc. Pet. Geol. Bull.* **69**, 1208–1216 (1985).

33. E. Dallmann, W. Gjelberg, J. Harland, W. Johannessen, H. B. Keilen, A. Lonoy, I. Nilsson, D. Worsley, "Upper Palaeozoic lithostratigraphy" in *Lithostratigraphic Lexicon of Svalbard: Review and Recommendations for Nomenclature Use: Upper Palaeozoic to Quaternary Bedrock*, W. K. Dallman, Ed. (Norsk Polarinstitutt, 2004), pp. 29–65.

34. S. S. Zeichner, J. Nghiem, M. P. Lamb, N. Takashima, J. de Leeuw, V. Ganti, W. W. Fischer, szeichner/Flocs-Code-and-Models: flocs1.1. Zenodo (2020); https://doi.org/10.5281/zenodo.4033293.

35. A. Ito, R. Wagai, Global distribution of clay-size minerals on land surface for biogeochemical and climatological studies. *Sci. Data* **4**, 170103 (2017). doi:10.1038/sdata.2017.103

36. R. L. Wershaw, "Evaluation of conceptual models of natural organic matter (humus) from a consideration of the chemical and biochemical processes of humification" (Report 5121, U.S. Geological Survey, 2004).

37. C. F. Wang, X. Fan, F. Zhang, S. Z. Wang, Y. P. Zhao, X. Y. Zhao, W. Zhao, T. G. Zhu, J. L. Lu, X. Y. Wei, Characterization of humic acids extracted from a lignite and interpretation for the mass spectra. *RSC Advances* **7**, 20677–20684 (2017). doi:10.1039/C7RA01497J

38. M. Lupker, C. France-Lanord, J. Lavé, J. Bouchez, V. Galy, F. Métivier, J. Gaillardet, B. Lartiges, J.-L. Mugnier, A Rouse-based method to integrate the chemical composition of river sediments: Application to the Ganga basin. *J. Geophys. Res.* **116**, F040124 (2011). doi:10.1029/2010JF001947

39. V. Galy, B. Peucker-Ehrenbrink, T. Eglinton, Global carbon export from the terrestrial biosphere controlled by erosion. *Nature* **521**, 204–207 (2015). doi:10.1038/nature14400 Medline

40. B. Le Quéré *et al*., Global Carbon Budget 2018. *Earth Syst. Sci. Data* **10**, 2141–2194 (2018). doi:10.5194/essd-10-2141-2018

41. A. N. Kolmogorov, The local structure of turbulence in incompressible viscous fluid for very large Reynolds numbers. *Proc. R. Soc. London Ser. A* **434**, 9–13 (1991). doi:10.1098/rspa.1991.0075

42. R. King, Ed., *Fluid Mechanics of Mixing: Modelling, Operations and Experimental Techniques* (Springer, 1992).

43. M. P. Lamb, B. McElroy, B. Kopriva, J. Shaw, D. Mohrig, Linking river-flood dynamics to hyperpycnal-plume deposits: Experiments, theory, and geological implications. *Bull. Geol. Soc. Am.* **122**, 1389–1400 (2010). doi:10.1130/B30125.1

44. G. Parker, M. Garcia, Y. Fukushima, W. Yu, Experiments on turbidity currents over an erodible bed. *J. Hydraul. Res.* **25**, 123–147 (1987). doi:10.1080/00221688709499292

45. G. Parker, Self-formed straight rivers with equilibrium banks and mobile bed. Part 1. The sand-silt river. *J. Fluid Mech.* **89**, 109–125 (1978). doi:10.1017/S0022112078002499

46. C. Paola, V. R. Voller, A generalized Exner equation for sediment mass balance. *J. Geophys. Res. Earth Surf.* **110**, F04014 (2005). doi:10.1029/2004JF000274

47. B. P. R. Jordan, "Fluvial sediment of the Mississippi River at St. Louis, Missouri" (Water Supply Paper 1802, U.S. Geological Survey, 1965).

48. C. H. Scott, H. D. Stephens, "Special sediment investigations: Mississippi River at St. Louis, Missouri, 1961–63" (Water Supply Paper 1819-J, U.S. Geological Survey, 1966).

49. M. G. Wolman, L. B. Leopold, "River flood plains: Some observations on their formation" (Geological Survey Professional Paper 282–C, U.S. Government Printing Office, 1957), pp. 87–107.

50. R. I. Ferguson, M. Church, a simple universal equation for grain settling velocity. *J. Sediment. Res.* **74**, 933–937 (2004). doi:10.1306/051204740933